




Kink-free electrospun PET/PU-based vascular grafts with 3D-printed additive manufacturing reinforcement

Kiran R. Adhikari^{1,2}, Jordan Zimmerman³, Pravin S. Dimple⁴, Bernabe S. Tucker⁴,
Vinoy Thomas^{2,4,a} 

¹Department of Physics, University of Alabama at Birmingham, Birmingham, AL 35294, USA

²Center for Nanoscale Materials and Biointegration (CNMB), University of Alabama at Birmingham, Alabama, USA

³Department of Chemical, Biological, and Materials Engineering, University of Oklahoma, Norman, USA

⁴Department of Materials Science and Engineering, University of Alabama at Birmingham, Birmingham, AL 35294, USA

^aAddress all correspondence to this author. e-mail: vthomas@uab.edu

Received: 26 February 2021; accepted: 28 June 2021; published online: 9 July 2021

In this study, we present the fabrication and characterization of the kink-free electrospun small caliber (4 mm in internal diameter) vascular graft based on a blend of biocompatible poly(ethylene terephthalate) (PET) and highly elastomeric polyurethane (PU) and subsequently reinforced by additive manufacturing 3D printing. We also report the design and simulation of the grafts under various internal pressures. Long-length small-diameter grafts suffer from the kink and loop formation for electrospun tubes. We have seen that collector rotation speeds (from 50 to 200 rpm) yielded grafts with varied mechanical properties and kink resistance. By reinforcing electrospun vascular grafts with the help of 3D printing, we report the reduction of the kink radius from 2.30 to 0.45 cm and 0.57 cm, respectively, for poly(lactic acid) (PLA)- and PET-reinforced vascular graft.

Introduction

The number of people affected by cardiovascular diseases (CVDs), often defined as conditions that affect the heart and/or the vascular systems of the body, is growing every year in the world, and so are the deaths, making CVDs one of the major causes of death and diseases [1, 2]. An estimated 17.9 million people died in 2016 from complications related to cardiovascular disease, which was 31% of all deaths in the world that year according to WHO [3]. These deaths are often avoidable and happen prematurely before the age of 70 and yet the number of CVD cases and deaths are likely to increase over the years.

Peripheral arterial disease (PAD) is one of the major cardiovascular conditions along with strokes, coronary arterial disease, and aortic disease. PAD leads to restricted or reduced blood flow to the extremities of limbs leading to failure of circulation of oxygenated blood to the extremities [4, 5]. This reduced flow in PAD as the plaque develops in the blood vessels leading to a condition called atherosclerosis and over time the plaque hardens and ultimately results in stiff arteries and narrowing of blood vessels [6]. Although interventions like increased exercises, cessation of smoking, other habitual changes, and drugs can bring

symptomatic relief to the patient, loss of limbs is a major risk to the patients [7].

Along with other interventions the treatment of CVDs, and specifically PAD, often requires the replacement of blood vessels in the patient's body. In the USA alone, 1.4 million patients require arterial prosthesis to treat their conditions [8, 9]. Various biological candidates are proposed for the replacement of the vascular grafts such as autografts, allografts, and xenografts, each having different shortcomings like a dimensional mismatch, donor site morbidity, immune rejection from the body, limited supply, and inferior mechanical properties [10–12]. All of these grafts being biological systems have limited to no control over the dimensional tunability, physical properties, and manufacturing.

Despite years of research, long-term patency is a greater issue in the case of grafts with a small or medium diameter (<6 mm) due to the development of thrombosis, stenosis, occlusion, and hyperplasia in the implanted grafts [9, 10, 13, 14]. The reasons for the development of these complications can be attributed to factors such as (1) the mechanical mismatch between the natural vessel of the host body and the implanted

graft leading to the compliance mismatch [9, 10, 15] and (2) lacking the biomimicry of the environment of the graft compared to natural vessels [16]. Also, the failure of the implanted grafts is associated with the poor mechanical properties of the replacement graft. The graft efficacy is compromised due to the development of complications like intimal hyperplasia and accelerated atherosclerosis [17]. Plaque development inside the wall of the implanted graft or the early sign of the thrombogenic development goes undetected until it is too late and there is no good solution available [18, 19].

Electrospinning is a well-known method used to fabricate a seamless conduit in vascular graft research and has a tremendous advantage in that it can be used to produce fibers and meshes that have comparable structure and morphology to the collagen in the natural extracellular matrix (ECM). It can be used for a myriad of materials and has excellent control over the process parameters [20, 21]. Researchers over the year reported the fabrication of vascular grafts from natural, biological, and synthetic materials or the combination of them and reported promising results [22–24]. Various biocompatible polymers like polyethylene terephthalate (PET), polycaprolactone (PCL), poly(lactic acid) (PLA), polyurethane (PU) and their blends have been reported examining different mechanical, morphological, and biological properties [25–31]. Hasan et al. studied the blend of PET and PU for the vascular graft application in their 2015 study and reported the mechano-morphological properties for different blending ratios [32]. PET is a well-known material used in the fabrication of synthetic graft commercially known as Dacron and is being used in vascular surgeries for years [33]. PU, on the other hand, is an elastomer widely used for biomedical applications. Both materials have been used in large diameter vascular grafts and are biocompatible materials. [34]

Similarly, 3D printing, or additive manufacturing, has garnered significant interest over the past few decades [21]. In the realm of tissue engineering, 3D printing has been explored for its potential to create precise designs for myriad applications and has been utilized for the creation of versatile tissue scaffolds that exhibit favorable and customizable biomechanical properties [35, 36]. Most of the 3D-printed vascular graft application research involves patient-specific graft fabrication and mostly used as scaffolds. This approach is mainly regarded as a promising candidate for the next-generation class of tissue-engineered vascular grafts. Kabirian et al. reported the fabrication and characterization of PLA-based 3D-printed vascular grafts which degrade as the tissue regeneration takes place [37]. Rabionet et al. reported the fabrication and determined the effect of various process parameters in cell proliferation [38]. But much research and improvement are required in order to develop viable artificial blood vessels [39]. PET and PLA are thermoplastic crystalline polymers with extrusion printability

for creating spirals around the electrospun graft for kink resistance reinforcements. PET is a biostable polymer and PLA is having half-life of more than 2 years with proven biocompatibility as sutures. The materials used for 3D printing were PLA and PET since both of these materials offer different advantageous properties like superior mechanical properties, ease of 3D printability and biocompatibility, etc. that make them excellent material choices for vascular grafts [40, 41]

Despite having much interest and ongoing research, the currently 3D-printed grafts lack the necessary porous structure vital for the long-term patency of the grafts. On the other hand, the replacement of vessels for treating PAD is generally longer length bypasses which suffer from physical occlusion of blood flow due to the kinking observed at the bending and joints [42]

Therefore, in this study, we explore a novel technique to combine electrospinning and 3D printing methods to develop a vascular graft system with mechanical properties comparable to the native blood vessels, possessing a structure that mimics the extracellular matrix of the native vessels, and is kink resistant. The patient population with PAD that requires surgical intervention is approximately 100,000 cases annually and additional cases involving multiple revascularization procedures would be the immediate beneficiaries of a “ready to implant off-the-shelf” vascular substitute (<6 mm diameter).

Results

Morphological characterization

Figure 1 presents the SEM imaging of the grafts and the diameter distribution of the fibers in the electrospun layer. Figure 1a shows the cross-sectional bilayer view of the graft, with the right solid layer representing the 3D-printed filament layer, and the left layer representing the electrospun PET/PU layer. There is good contact and lamination between the electrospun layer and the 3D-printed layer as seen in the SEM image, allowing for a combination resulting from the novel incorporation of electrospinning and additive manufacturing. Figure 1b depicts the SEM image of the outer side of the graft showing even spacing between the filaments over the electrospun inner layer.

SEM images of PET/PU electrospun grafts depicted in Fig. 1c show the randomly oriented fibrous mat with the high porosity ($79.29 \pm 4.19\%$, $n = 5$) associated with electrospun fibers. The image depicts the highly connected electrospun fiber mats. The diameter distribution analysis as shown in Fig. 1d shows that the majority of the fibers are below 500 nm in diameter. DiameterJ (free software from NIH) measurements confirmed that fiber diameters were on the order of collagen fibers of the ECM: 54.6% of diameters fell between 120 and 365 nm, while 78% of diameters fell between 50 and 500 nm.

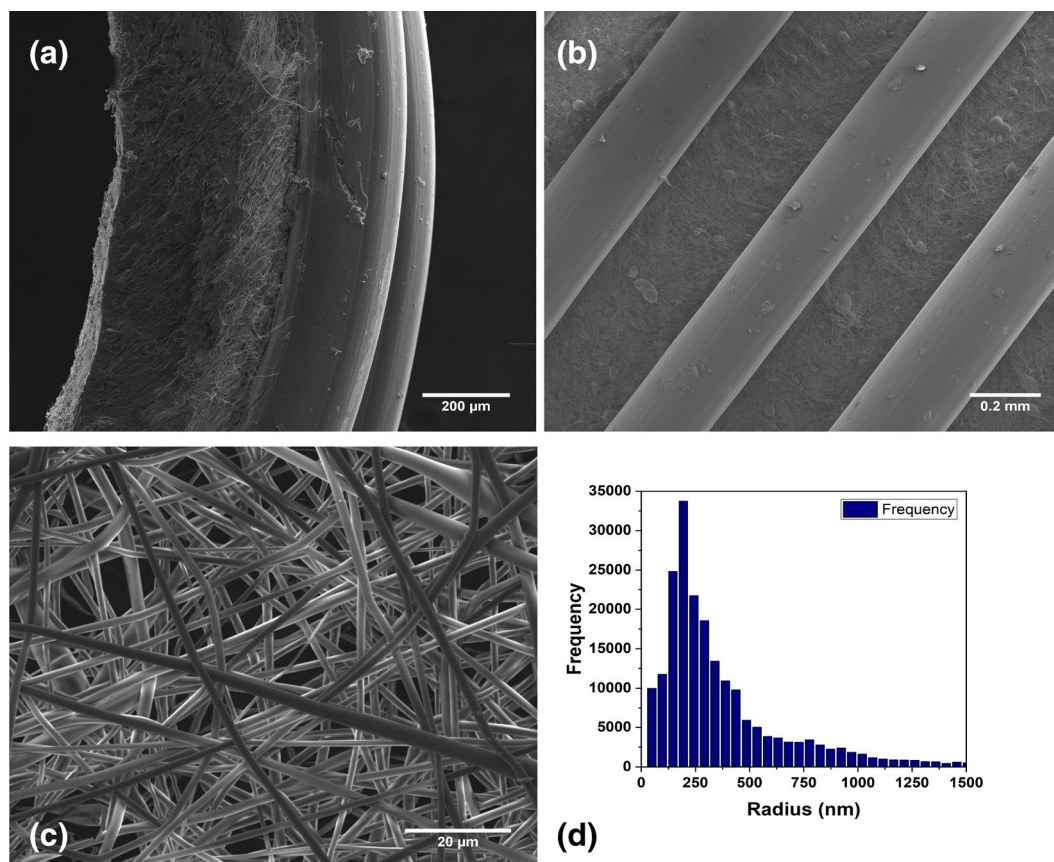


Figure 1: SEM images of the grafts. (a) cross-sectional view showing both the filament and electrospun layer. (b) front view of the graft. (c) electrospun PET/PU layer. (d) diameter distribution of the fibers in the electrospun layer.

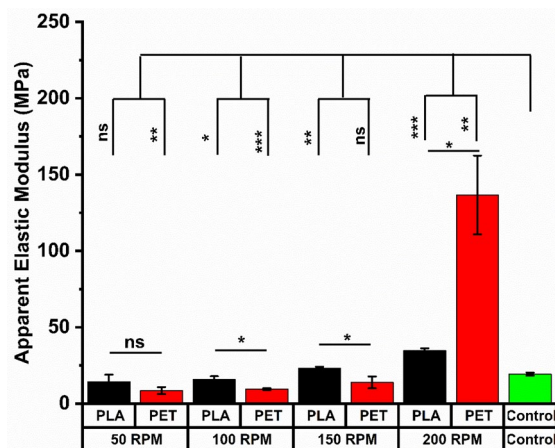


Figure 2: Apparent elastic modulus of the electrospun grafts with the 3D reinforcement using PLA and PET as filaments at the different collector rotation speed ($n=3$ per group, $*p \leq 0.05$, $**p \leq 0.01$, $***p \leq 0.001$) and control being electrospun grafts without 3D reinforcement.

FTIR surface chemistry

The FTIR spectrum shown in supplementary data, SP 2c, was performed on a sample of electrospun PET/PU graft (control). As is

expected from the given polymers used, a $-OH$ and $N-H$ peak can be observed in the broad region ($\sim 3600-3000 \text{ cm}^{-1}$), $-CH_2$ peaks appeared at around wavenumbers $2900-2800 \text{ cm}^{-1}$, and a prominent $-C=O$ peak is depicted at 1724 cm^{-1} associated with urethane carbonyl of PU with shoulder ester carbonyl of PET. Finally, $-C-O-C$ and other single-bonded functional groups can be found in the $1400-1000 \text{ cm}^{-1}$ region, which is associated with the ester/urethane ether group.

Mechanical properties

The apparent elastic modulus of the grafts with the intact cylindrical geometry is measured and the apparent tensile modulus of the grafts is represented in Fig. 2. The schematic of the test coupon and method is shown (Supplementary data, SP 1). The graph shows the apparent elastic modulus of the grafts post 3D printing and is compared to the electrospun control graft. The apparent elastic modulus for the control graft measured to be $19.3 \pm 1.06 \text{ MPa}$ and that for PET-reinforced grafts at 50 RPM, 100 RPM, 150 RPM, and 200 RPM was found to be $8.51 \pm 2.31 \text{ MPa}$, $9.51 \pm 0.61 \text{ MPa}$, $13.9 \pm 3.87 \text{ MPa}$ and $137 \pm 25.8 \text{ MPa}$, respectively. Similarly for PLA-reinforced

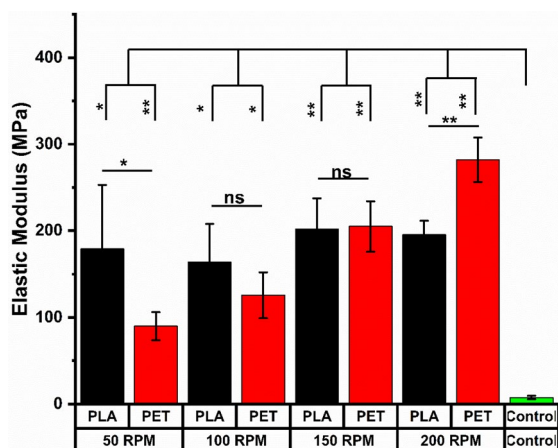


Figure 3: Elastic modulus in the circumferential direction ($n=3$ per group, $*p \leq 0.05$, $**p \leq 0.01$) of control electrospun grafts, and PLA and PET (with different RPMs) grafts with 3D-printed reinforcement.

grafts, the values for 50 RPM, 100 RPM, 150 RPM, and 200 RPM were found to be 14.3 ± 4.6 MPa, 15.7 ± 2.2 MPa, 23.1 ± 1.07 MPa, and 34.7 ± 1.51 MPa, respectively.

Figure 3 represents the elastic modulus of the graft in the circumferential direction. The graft was cut open, and the modulus

is measured following the ASTM standard. The graph and the value show that there is a significant increase in the elastic modulus in the circumferential direction post 3D printing. The elastic moduli in the circumferential direction for the control grafts measured to be 7.43 ± 1.99 MPa and that for PET-reinforced grafts at 50 RPM, 100 RPM, 150 RPM, and 200 RPM was found to be 90.0 ± 16.2 MPa, 126 ± 26.5 MPa, 205 ± 29.1 MPa and 282 ± 25.6 MPa, respectively. Similarly for PLA-reinforced grafts, the values for 50 RPM, 100 RPM, 150 RPM, and 200 RPM were found to be 179 ± 73.5 MPa, 164 ± 43.8 MPa, 202 ± 35.4 MPa, and 195.3 ± 16.7 MPa, respectively.

Kink radius measurement

Figure 4a represents the measured kink radius of the grafts. Kink radius as measured by bending from both ends of grafts until noticeable bends or kinks formed show there is an improvement in the kink radius. The kink radius of the control graft was measured to be 2.30 ± 0.19 cm. The least kink radius is reported in the PLA-reinforced graft at 50 RPM and measured as 0.45 ± 0.02 cm and that for PET-reinforced graft at 50 RPM is measured as 0.57 ± 0.02 cm. Figure 4b represents the fabricated

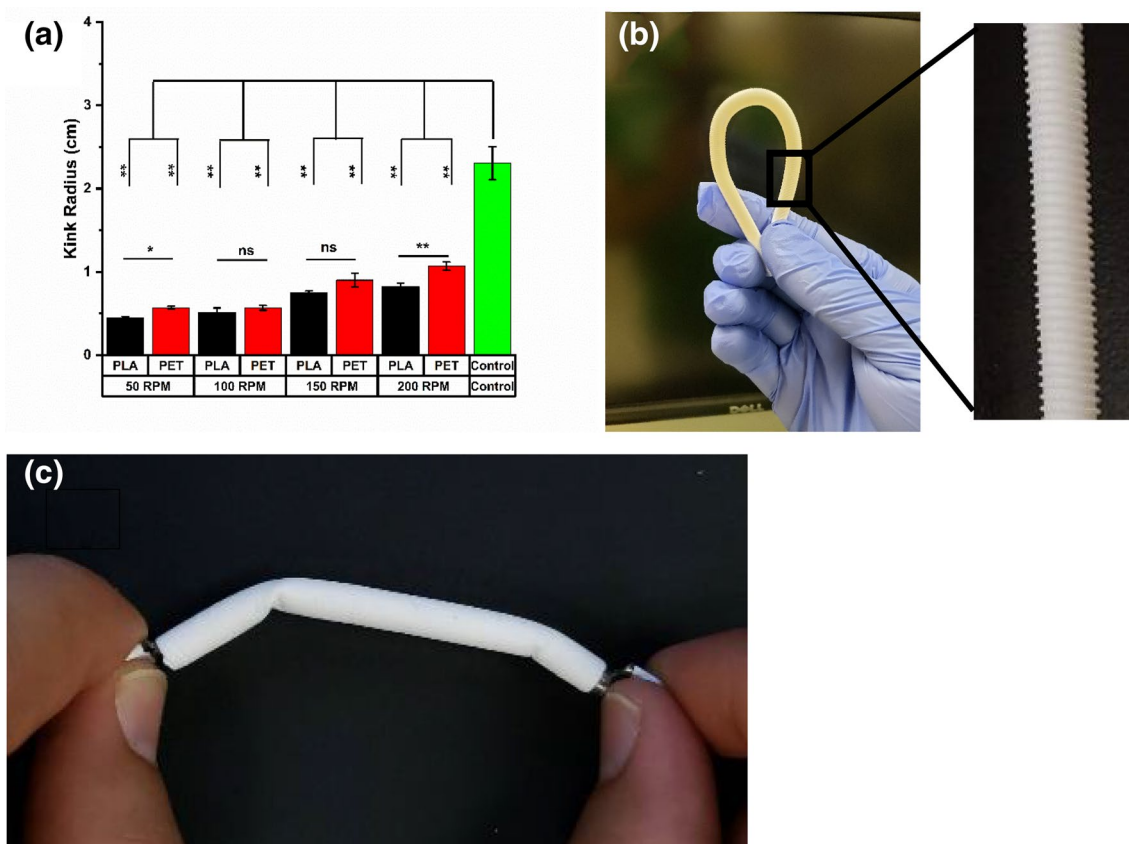


Figure 4: (a) Distribution of kink radii of samples as measured by fitting circles to inner diameters using ImageJ. (b) kink-free graft fabricated with electrospinning and 3D printing. (c) Kinking nature of electrospun graft without 3D printing reinforcement (control). ($n=3$ per group, $*p \leq 0.05$, $**p \leq 0.01$).

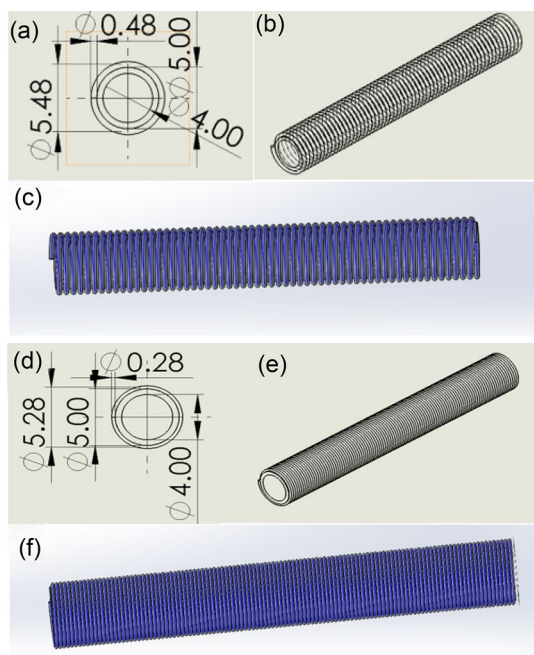


Figure 5: Graft design in SOLIDWORKS for simulation. (a) Top view of the graft. (b) 3D view of the graft. (c) 3D CAD design of graft prepared at 50 RPM. (d) Top view of graft. (e) 3D view of the graft. (f) 3D CAD design of graft prepared at 100 RPM.

graft by both electrospinning and those reinforced by 3D printing for kink-resistance.

Burst pressure measured for the electrospun control grafts was found to be 1787.64 ± 76.61 mm of Hg ($n = 3$). For grafts with reinforcements, the grafts did not burst until the limitation of the setup and the burst strength was achieved at an average value of 2650 mm of Hg where the experiment was stopped.

TABLE 1: Stress, Strain, and Displacement of the tube under different pressures prepared at 50RPM (from Simulation).

Pressure (mm of Hg)	Stress (N/m ²)	Strain	Deformation/displacement (mm)
80	5.881e+04	1.492e-05	3.486e-05
100	7.464e+04	1.886e-05	4.461e-05
120	8.956e+04	2.264e-05	5.353e-05
140	1.045e+05	2.641e-05	6.245e-05
180	1.343e+05	3.396e-05	8.030e-05
250	1.866e+05	4.716e-05	1.115e-04
300	1.087e+06	2.334e-04	1.221e-04
500	1.449e+06	1.629e-04	3.11e-04
1000	3.662e+06	7.782e-04	4.071e-04
1500	3.797e+06	9.324e-04	7.019e-04
2000	5.062e+06	1.242e-03	9.35e-04

TABLE 2: Stress, Strain and Displacement of the tube under different pressures prepared at 100RPM (from simulation).

Pressure (mm of Hg)	Stress (N/m ²)	Strain	Deformation/displacement (mm)
80	5.675e+04	1.378e-05	3.183e-05
100	7.094e+04	1.722e-05	3.979e-05
120	8.513e+04	2.066e-05	4.774e-05
140	9.932e+04	2.411e-05	5.570e-05
180	1.277e+05	3.099e-05	7.161e-05
250	1.774e+05	4.305e-05	9.947e-05
300	2.191e+05	5.516e-05	1.349e-04
400	2.992e+05	7.354e-05	1.799e-04
500	3.684e+05	9.493e-05	2.315e-04
1000	7.368e+05	1.899e-04	4.630e-04
1500	1.105e+06	2.848e-04	9.945e-04
2000	1.474e+06	3.797e-04	9.260e-04

Design using SOLIDWORKS

Figure 5 represents the design for 50 RPM and 100 RPM grafts. The dimension of the filament was measured from the SEM images included in the supplementary materials SP2. The internal diameter of the design was 4 mm and the outer diameter with the filaments was 5 mm. Figure 5a–c represent the top view, 3D design, and 3D CAD design of the 50 RPM graft and Fig. 5d–f represent the top view, 3D design, and 3D CAD design of the 100 RPM grafts.

Table 1 represents the values of the maximum stress, strain, and displacement developed under the various pressure inside the graft with 50 RPM reinforcements.

Table 2 represents the values of the maximum stress, strain, and displacement developed under the various pressure inside the graft with 100 RPM reinforcements.

The stresses in both the graft models increase as the pressure increases. The values for stresses, strains, and the deformation in the graft made with 50 RPM reinforcement have shown to have a higher value than the graft made with 100 RPM reinforcement. The maximum stress developed are 0.186 MPa and 0.177 MPa for 50 RPM grafts and 150 RPM grafts at 250 mm of Hg internal pressure and the maximum strain for the same grafts was $4.716e-05$ and $4.305e-05$, respectively. Additional simulations were performed at higher pressure values with reference to the burst pressure of the human saphenous vein, 1599 ± 877 mm of Hg, reported by various researchers [43–45].

Discussion

In this study, we report the fabrication of a kink-free synthetic graft by a novel combination of electrospinning and 3D printing. Electrospinning can easily be used to synthesize seamless tubular structures of any diameter and length. These grafts also do not have the flexibility over the long length as a vascular replacement since they form kinks. Some other studies include printing grafts by additive manufacturing methods only producing very stiff grafts not suitable for clinical uses. Poly(ethylene terephthalate) (PET), a known synthetic vascular graft polymer (Dacron), was blended with highly elastic biostable and biocompatible silicon-based polyurethane (PU-E2A from AorTech International) to synthesize the inner layer. By blending stiff PET with highly elastic PU by co-spinning and the combination with 3D-printed spirals could impart strength, flexibility, and kink resistance to the graft. Moreover, the addition of PU with rubbery visco-elasticity attribute could give suture puncture healing effects.

By fabricating the inner layer of the graft by the electrospinning process, we report the highly porous fiber-mesh of interconnected pores in the interior of the grafts resembling the structure of the ECM morphology of the natural blood vessels. This structure is a must for the development of smooth endothelial lining onto the luminal surface of the graft [21, 46]. The majority of the fibers in the electrospun layer have a diameter that is comparable to the diameter distribution of collagen fibers found in the natural blood vessels. Mimicking the physical structure of the collagen fibers in the blood vessels is very essential in the long-term patency of the grafts as the biomimetic microenvironment is very important in cell development and proliferation [47]. The collagen in the ECM have sizes in the range of 50–500 nm [48, 49]. The diameter analysis of the SEM image of the electrospun layer shows 78% of the fibers lie in this range (Fig. 1). SEM images showing the fiber size of electrospun pure PU and PET and chemistry of blend by infrared spectroscopy (IR) can be seen in Supplementary data (SP 2). These IR peaks are observed due to the functional groups of PET/PU that are attributed to the signature peaks associated with the individual polymers used and are consistent with the results obtained by Khodadoust et al. using PET and PU for the graft fabrication [34].

The SEM images also reveal a good contact and lamination between the electrospun layer and the 3D-printed filament (Fig. 1) which suggests its integrity in the cyclic environment of the blood vessels during the systolic and diastolic cycle of the blood flow. This lamination occurred as a result of the heat applied to the 3D-printed filament, which comes out hot from the extruder head, assisting the bonding between these layers.

The kink radius is reduced significantly for the reinforced grafts compared to the control grafts made with electrospinning

only. All the grafts reinforced with 3D-printing filaments have less than half the kink radius of the control grafts. The best improvement measured was for the PLA-reinforced graft at 50 RPM, which is less than one-fifth of the kink radii of the control graft, which are 0.45 ± 0.02 cm and 2.30 ± 0.19 cm, respectively, closely followed by PET-reinforced graft at 50 RPM, whose kink radius is measured to be 0.57 ± 0.02 cm. SEM images of the reinforced graft can be seen in Fig. 1 and Supplementary data SP 3. Most reinforced grafts did not kink in the traditional sense of the word; rather, they experienced bending that would likely still allow for flow to continue mostly uninterrupted. Additionally, they offered more resistance to bending than control grafts, meaning that, in addition to having smaller kink radii, more force would be required to reach those points than for control grafts. Notably, the PLA-reinforced graft at 50 RPM did not kink or bend at all, and thus, the noted kink radius is that of the minimum radius reached via the testing method used.

The elastic modulus measurement is done in two different ways: apparent elastic modulus in the longitudinal direction and elastic modulus in the circumferential direction. From the results of both these tensile measurements, we can conclude that the electrospun layer mostly dictates the elastic strength in the longitudinal direction, while the elastic modulus in the circumferential direction is dictated by the 3D-printed filament layers. The apparent elastic modulus in the longitudinal direction for the reinforced, on average, has values comparable to the electrospun control grafts. We expected heat during the 3D printing process and the lamination during this process would melt some electrospun fibers and would decrease the elastic modulus in the longitudinal direction. The reason filament layers would not have much influence on the elastic properties in the longitudinal direction is they form a spiral around the conduits and results in an increase in the distance between the filaments subjected upon the force in the direction, hence load is transferred mostly in the electrospun layer. There is a sharp increase in the apparent elastic modulus for grafts with PET reinforcement at 200 RPM. This can be attributed to the fusing of some adjacent filaments due to the higher printing temperature for PET printing and the nature of the PET filament used. With exception to the grafts at 200 RPM, PLA-reinforced grafts had, on average, higher apparent modulus which can be attributed to the higher extrusion temperature of PET printing (220 °C) compared to that of PLA (190 °C) printing. The variation of the diameter and the distance between the two successive spirals (measured from SEM images) of the grafts produced at different collector rpm using ImageJ software is given Supplementary data (SP 4).

The elastic modulus in the circumferential direction has shown to have a significant increase in the case of reinforced grafts. Tensile test in the circumferential direction indicated that the elastic modulus in the circumferential direction was substantially higher than that of control grafts (Fig. 3) suggesting a

tangible improvement by combining 3D printing with electrospinning. This result is very important during the blood flow as the walls of the vessels act as the barrier that balances the hydrostatic pressure and the oncotic pressure through the vessel wall [50–52]. The mechanical properties and the modulus values are found to be higher compared to the natural blood vessels. For example, the elastic modulus values for the saphenous vein in the circumferential direction is reported to be 43 MPa [53], 4.2 MPa [54], and that for the femoral artery is reported to be in the range 9–12 MPa [55, 56]. These values are comparable to the values we report with the control graft (7.43 ± 1.99 MPa), the lowest among the graft fabricated, whereas other grafts show superior mechanical properties. Khodadoust et al. in their 2017 study reported the mechanical properties of the PET-PU hybrid grafts and cytotoxicity of the grafts has been evaluated in with MTT assay for human skin fibroblast cells and found to be non-toxic to the cells [34].

The control electrospun PET-PU graft shows a burst pressure of 1787.64 ± 76.61 mm of Hg (Supplementary data SP 5) which is comparable to the saphenous vein's burst pressure (~ 1800 mm Hg) described in the literature [44]. The reinforced grafts were able to withstand more than 2500 mm Hg that they did not burst even at higher pressures (2650 mm of Hg). The reinforced grafts had much higher burst strength than that of the non-reinforced graft (control) or the natural saphenous vein.

The simulation work represents the theoretical predictions to see how the grafts would behave in different pressure conditions. The results investigate the stress, strain, and deformation under various pressures, ranging from normal blood pressure to hypertension. The values obtained for stresses and strain are well below the stress and strain measured in the tensile tests performed in both longitudinal and circumferential directions. This result demonstrates the viability of these grafts for vascular graft applications as they would be able to perform well under the systolic and diastolic pressure inside the blood vessel. This simulation work is performed for the PET-reinforced graft, but the design can be used for other materials with known mechanical properties. This study includes the simulation work for the lower RPM grafts due to the limit of the SOLIDWORKS node limit for mesh structure.

Conclusions

By harnessing electrospinning with the additive manufacturing technique such as 3D-printing process, we fabricated a bi-layer vascular graft with superior mechanical properties, notably in the circumferential direction. These layers have excellent lamination and kink resistance with ECM-like internal mesh structure

mimicking natural blood vessels. Fabricating kink-resistant vascular grafts is advantageous for future synthetic vascular graft developments, especially for grafts with long lengths and small diameters. The simulation results suggest that these grafts will withstand the pressure behavior inside the blood vessels.

Further studies could include experimenting with a range of materials and geometries for producing grafts with matching mechanical properties by combining 3D printing and electrospinning. However, the patency should be ultimately assessed by the biocompatibility of grafts under in vitro and preclinical in vivo conditions. We have previously shown that atmospheric pressure plasma jet could selectively functionalize the luminal surface of small caliber tubes for improved blood compatibility [31, 32].

Materials and methods

Graft preparation

Electrospinning

An 18% wt/vol of polymer blend was prepared by dissolving PET and PU (4:1 ratio) in 1,1,1,3,3,3-hexafluoro-2-propanol (HFIP). PET was stirred in HFIP for 48 h before adding the PU and then they were stirred further for 24 h. The parameter for the electrospinning set is as follows: the voltage 20 kV, needle to collector distance 20 cm, and flow rate 1 mL/h. The collector for the electrospinning process was a rotating stainless steel mandrel of diameter 4 mm rotating at 600 RPM (0.126 m/s), resulting in grafts with an internal diameter of 4 mm. The total volume of the solution used for the preparation of each conduit was 2 ml. The flow rate was maintained throughout the electrospinning process by using Harvard PHD 2000 Advanced syringe pump.

3D printing

Once the electrospinning step is concluded the grafts were externally reinforced with 3D printing. 3D printing is carried by moving the extruder head at a constant rate, while the mandrel containing the electrospun graft was rotating at different speeds. The filaments used for the reinforcements were PLA and PET and both are extruded at the rate of 1 mm/s of 1.75 mm diameter filaments. The lateral distance the extruder head moved was 140 mm at 1mm/s speed resulting in 15-cm-long reinforced grafts. The collecting mandrel was rotated at different rotating speeds—50 RPM, 100 RPM, 150 RPM, and 200 RPM resulting in grafts with different reinforcement properties.

The mandrels after 3D printing were then ultrasonicated in the water bath for 2 h and then grafts were removed from the mandrel and dried in the vacuum desiccator for 48 hours to be ready for further analysis.

Characterization

Morphological characterization

The structure and the morphological analysis of the graft, both electrospun layer and the 3D-printed layer, was first sputter-coated with Au–Pd, and imaging was done with FE-SEM (Quanta FEG 650 from FEI, Hillsboro, OR USA) at different magnifications and further measurements were done using ImageJ (NIH).

Porosity measurement

The porosity of the grafts was measured by using the liquid intrusion method. The samples were cut into squares of 1 cm × 1 cm in size, $n = 5$, and weighted before emerging in ethanol under ultrasonication. After 30 min, the samples were patted dry and weighted again, the weight is converted to volume by using the density of the ethanol at room temperature to calculate the porosity using the following formula:

$$\text{Porosity} = \frac{\text{Volume of ethanol diffused}}{\text{Total volume of the samples}} \times 100 \%$$

Mechanical characterization

To evaluate the mechanical properties of the graft in the longitudinal and circumferential direction, the samples were tested using a DMA analyzer (TA Instruments, RSA G2) in tension mode under constant stress.

Tensile testing -longitudinal direction

Apparent elastic modulus was measured using the modified setting according to the protocol described in the literature [57]. The cylindrical samples were clamped with the modified setup to measure the apparent elastic modulus in the longitudinal direction. The samples were 35 mm in length, and $n = 3$ for each sample was taken. The thickness of the electrospun layer of the samples was 0.45 ± 0.06 mm.

Tensile testing- circumferential direction

For circumferential tensile measurements, grafts were cut open to form strips of reinforced plastic that were then mounted in the DMA machine using a standard set up according to the ASTM D882 standard for tensile testing of thin-film plastics [58]. The length of the samples was 12.6 cm and the average width of the samples was 4.5 ± 0.6 mm, $n = 3$.

Apparent elastic moduli and elastic moduli were evaluated for grafts by obtaining the slope of the elastic region of the stress–strain curves accompanying each graft. Tensile testing was performed in dry conditions at constant strain mode at room temperature.

Kink radii were evaluated by bending from both ends of grafts until noticeable bends or kinks formed that could occlude flow [59, 60]. Then, several points were demarcated about the grafts at the point of bending/kinking. ImageJ (NIH) analysis allowed for the fitting of arcs along the points to properly evaluate kink radius.

Burst pressure measurement was evaluated for grafts using Eisco NeuLog Pressure Logger Sensor—Recorders with NeuLog USB connection module. The graft being highly porous, the catheter balloon method was used. The procedure for using a catheter balloon to measure is outlined in ISO 7198:1988 and is described in Jones et al. studies [61]. A 30 ml syringe(BD) was used and a pump was used to maintain a flow of 4 ml/min and the pressure was recorded using the NeuLog module. A 3.5-cm-long section of the graft was directly mounted on the top of Foley catheter FR12 and the pump was run. The test was run until the graft ruptured or the pressure plateaued due to the physical constraints of the catheter, tubing, connection, and syringe pump.

Statistical analysis was performed using a t-test: two-sample using unequal variance between the groups. A statistical level of p -value < 0.05 was considered a significant difference. All the values are represented as mean value \pm standard deviation.

Simulation for stress, strain, and deformation

The model of the grafts was designed with the help of SOLIDWORKS Inc 2019–2020 and ANSYS software, simulations were run for the determination of stress, strain, and deformation developed at various internal pressure. After measuring all the required dimensions of grafts prepared at different rpm, 3D design was done using the SOLID Works Inc 2019–2020; for the simulation it was necessary to convert SOLID Works design files into IGES format, because ANSYS accepts external files in the.IGES format. Although the design is possible in ANSYS due to the complexity of grafts, the use of SOLIDWORKS for design is preferred. The values for the exact dimensions for the simulation work were done using the SEM image analyzed by ImageJ (Supplementary data SP 4). The filament materials for the simulation purpose were chosen to be PET and standard PET materials properties were used to perform such simulation. Even though PET is used for the simulation, once the model was developed, only changing the properties value could be used to simulate for other materials (PLA) for the same geometry. These simulations were performed for the grafts made at 50 RPM and 100 RPM, and the mesh structure for higher RPM grafts was not supported by the mesh limit of the SOLIDWORKS software.

Acknowledgments

Funding support was provided by Alabama EPSCoR GRSP round 14 and 15 Fellowship (KA) and NSF EPSCoR RII Track-1 OIA 1655280 (VT), and National Aeronautics and Space Administration (NASA)-Alabama Space Grant Consortium, Research Experiences for Undergraduates (REU) award (JZ) is acknowledged. Thanks to Mr. Jerry Sewell from Dept. of Physics, University of Alabama at Birmingham for assistance in the modification of the mechanical testing system. We greatly appreciate the elastomeric PU materials gifted by AorTech International Inc (Australia) for the studies.

Data availability

Data can be provided by the corresponding author upon request.

Declarations

Conflict of interest Authors have no conflict of interest.

Supplementary Information

The online version contains supplementary material available at <https://doi.org/10.1557/s43578-021-00291-6>.

References

1. K. McNamara, H. Alzubaidi, J.K. Jackson, Cardiovascular disease as a leading cause of death: how are pharmacists getting involved? *Integr. Pharm. Res. Pract.* **8**, 1–11 (2019). <https://doi.org/10.2147/IPRPS133088>
2. C.S. Higano, Cardiovascular disease and androgen axis-targeted drugs for prostate cancer. *N. Engl. J. Med.* **382**(23), 2257–2259 (2020). <https://doi.org/10.1056/NEJMe2016433>
3. Cardiovascular diseases (CVDs), WHO. [https://www.who.int/news-room/fact-sheets/detail/cardiovascular-diseases-\(cvds\)](https://www.who.int/news-room/fact-sheets/detail/cardiovascular-diseases-(cvds)). Accessed 05 Aug 2020
4. M. R. Zemaitis, J. M. Boll, M. A. Dreyer, Peripheral arterial disease, in *StatPearls*, Treasure Island (FL): StatPearls Publishing, 2020. <http://www.ncbi.nlm.nih.gov/books/NBK430745/>. Accessed 22 Feb 2021
5. A.W. Gardner, A. Afaq, Management of lower extremity peripheral arterial disease. *J. Cardiopulm. Rehabil. Prev.* **28**(6), 349–357 (2008). <https://doi.org/10.1097/HCR.0b013e31818c3b96>
6. Peripheral Artery Disease | NHLBI, NIH. <https://www.nhlbi.nih.gov/health-topics/peripheral-artery-disease>. Accessed 22 Feb 2021
7. K. Ouriel, Peripheral arterial disease. *Lancet* **358**(9289), 1257–1264 (2001). [https://doi.org/10.1016/S0140-6736\(01\)06351-6](https://doi.org/10.1016/S0140-6736(01)06351-6)
8. M.B. Browning et al., Multilayer vascular grafts based on collagen-mimetic proteins. *Acta Biomater.* **8**(3), 1010–1021 (2012). <https://doi.org/10.1016/j.actbio.2011.11.015>
9. A. Hasan et al., Electrospun scaffolds for tissue engineering of vascular grafts. *Acta Biomater.* **10**(1), 11–25 (2014). <https://doi.org/10.1016/j.actbio.2013.08.022>
10. S.J. Lee, J.J. Yoo, G.J. Lim, A. Atala, J. Stitzel, In vitro evaluation of electrospun nanofiber scaffolds for vascular graft application. *J. Biomed. Mater. Res. A* **83**(4), 999–1008 (2007). <https://doi.org/10.1002/jbm.a.31287>
11. K.R. Adhikari, B.S. Tucker, V. Thomas, 4 - Tissue engineering of small-diameter vascular grafts, in *Biointegration of Medical Implant Materials*, 2nd edn., ed. by C.P. Sharma (Woodhead Publishing, Sawston, 2020), pp. 79–100
12. C.-H. Lin, K. Hsia, H. Ma, H. Lee, J.-H. Lu, In vivo performance of decellularized vascular grafts: a review article. *Int. J. Mol. Sci.* **19**(7), 2701 (2018). <https://doi.org/10.3390/ijms19072101>
13. J.P. Stegemann, S.N. Kaszuba, S.L. Rowe, Review: advances in vascular tissue engineering using protein-based biomaterials. *Tissue Eng.* **13**(11), 2601–2613 (2007). <https://doi.org/10.1089/ten.2007.0196>
14. T.F. O'Donnell et al., Correlation of operative findings with angiographic and noninvasive hemodynamic factors associated with failure of polytetrafluoroethylene grafts. *J. Vasc. Surg.* **1**(1), 136–148 (1984). [https://doi.org/10.1016/0741-5214\(84\)90193-9](https://doi.org/10.1016/0741-5214(84)90193-9)
15. H. Inoguchi, I.K. Kwon, E. Inoue, K. Takamizawa, Y. Maehara, T. Matsuda, Mechanical responses of a compliant electrospun poly(L-lactide-co-epsilon-caprolactone) small-diameter vascular graft. *Biomaterials* **27**(8), 1470–1478 (2006). <https://doi.org/10.1016/j.biomaterials.2005.08.029>
16. S. Liao, B. Li, Z. Ma, H. Wei, C. Chan, S. Ramakrishna, Biomimetic electrospun nanofibers for tissue regeneration. *Biomed. Mater.* **1**(3), R45–53 (2006). <https://doi.org/10.1088/1748-6041/1/3/R01>
17. M.R. de Vries, P.H.A. Quax, Inflammation in vein graft disease. *Front. Cardiovasc. Med.* (2018). <https://doi.org/10.3389/fcvm.2018.00003>
18. M.D. Boisclair, H. Philippou, D.A. Lane, Thrombogenic mechanisms in the human: fresh insights obtained by immunodiagnostic studies of coagulation markers. *Blood Coagul. Fibrinolys* **4**(6), 1007–1021 (1993)
19. C.A. Labarrere, A.E. Dabiri, G.S. Kassab, Thrombogenic and inflammatory reactions to biomaterials in medical devices. *Front. Bioeng. Biotechnol.* (2020). <https://doi.org/10.3389/fbioe.2020.00123>
20. J. Xue, T. Wu, Y. Dai, Y. Xia, Electrospinning and electrospun nanofibers: methods, materials, and applications. *Chem. Rev.* **119**(8), 5298–5415 (2019). <https://doi.org/10.1021/acs.chemrev.8b00593>
21. S. Pashneh-Tala, S. MacNeil, F. Claeysens, The tissue-engineered vascular graft—past, present, and future. *Tissue Eng. Part B Rev.* **22**(1), 68–100 (2016). <https://doi.org/10.1089/ten.teb.2015.0100>

22. R. Huang et al., Triple-layer vascular grafts fabricated by combined E-Jet 3D printing and electrospinning. *Ann Biomed Eng* **46**(9), 1254–1266 (2018). <https://doi.org/10.1007/s10439-018-2065-z>
23. P.V. Popryadukhin et al., Tissue-engineered vascular graft of small diameter based on electrospun polylactide microfibers. *Int. J. Biomater.* **2017**, e9034186 (2017). <https://doi.org/10.1155/2017/9034186>
24. N.K. Awad, H. Niu, U. Ali, Y.S. Morsi, T. Lin, Electrospun fibrous scaffolds for small-diameter blood vessels: a review. *Membranes* (2018). <https://doi.org/10.3390/membranes8010015>
25. M.C. Burrows et al., Hybrid scaffolds built from PET and collagen as a model for vascular graft architecture. *Macromol. Biosci.* **12**(12), 1660–1670 (2012). <https://doi.org/10.1002/mabi.20120154>
26. D. Pezzoli, E. Cauli, P. Chevallier, S. Farè, D. Mantovani, Biomimetic coating of cross-linked gelatin to improve mechanical and biological properties of electrospun PET: a promising approach for small caliber vascular graft applications. *J. Biomed. Mater. Res. A* **105**(9), 2405–2415 (2017). <https://doi.org/10.1002/jbm.a.36098>
27. C.S. Wong, X. Liu, Z. Xu, T. Lin, X. Wang, Elastin and collagen enhances electrospun aligned polyurethane as scaffolds for vascular graft. *J. Mater. Sci. Mater. Med.* **24**(8), 1865–1874 (2013). <https://doi.org/10.1007/s10856-013-4937-y>
28. J.P. Theron et al., Modification, crosslinking and reactive electrospinning of a thermoplastic medical polyurethane for vascular graft applications. *Acta Biomater.* **6**(7), 2434–2447 (2010). <https://doi.org/10.1016/j.actbio.2010.01.013>
29. N. Jirofti, D. Mohebbi-Kalhari, A. Samimi, A. Hadjizadeh, G.H. Kazemzadeh, Small-diameter vascular graft using co-electrospun composite PCL/PU nanofibers. *Biomed. Mater.* **13**(5), 055014 (2018). <https://doi.org/10.1088/1748-605X/aad4b5>
30. F. Guo et al., An electrospun strong PCL/PU composite vascular graft with mechanical anisotropy and cyclic stability. *J. Mater. Chem. A* **3**(9), 4782–4787 (2015). <https://doi.org/10.1039/C4TA06845A>
31. J.D. Stitzel, K.J. Pawlowski, G.E. Wnek, D.G. Simpson, G.L. Bowlin, Arterial smooth muscle cell proliferation on a novel biomimicking, biodegradable vascular graft scaffold. *J. Biomater. Appl.* **16**(1), 22–33 (2001). <https://doi.org/10.1106/U2UU-M9QH-Y0BB-5GYL>
32. A. Hasan, G. Deeb, K. Atwi, S. Soliman, A. Hasan, Electrospun PET-PU scaffolds for vascular tissue engineering, in 2015 International Conference on Advances in Biomedical Engineering (ICABME), 2015, pp. 217–221. doi: <https://doi.org/10.1109/ICABME.2015.7323291>
33. S. Roll et al., Dacron® vs. PTFE as bypass materials in peripheral vascular surgery – systematic review and meta-analysis. *BMC Surg.* **8**, 22 (2008). <https://doi.org/10.1186/1471-2482-8-22>
34. M. Khodadoust, D. Mohebbi-Kalhari, N. Jirofti, Fabrication and characterization of electrospun Bi-Hybrid PU/PET scaffolds for small-diameter vascular grafts applications. *Cardio-vasc. Eng. Technol.* **9**(1), 73–83 (2018). <https://doi.org/10.1007/s13239-017-0338-6>
35. R.-D. Chen, C.-F. Huang, S. Hsu, Composites of waterborne polyurethane and cellulose nanofibers for 3D printing and bioapplications. *Carbohydr. Polym.* **212**, 75–88 (2019). <https://doi.org/10.1016/j.carbpol.2019.02.025>
36. B.-N.B. Nguyen, H. Ko, R.A. Moriarty, J.M. Etheridge, J.P. Fisher, Dynamic bioreactor culture of high volume engineered bone tissue. *Tissue Eng. Part A* **22**(3–4), 263–271 (2016). <https://doi.org/10.1089/ten.TEA.2015.0395>
37. F. Kabirian, B. Ditkowski, A. Zamanian, R. Heying, M. Mozafari, An innovative approach towards 3D-printed scaffolds for the next generation of tissue-engineered vascular grafts. *Mater. Today Proc.* **5**(7), 15586–15594 (2018). <https://doi.org/10.1016/j.matpr.2018.04.167>
38. M. Rabionet, A.J. Guerra, T. Puig, J. Ciurana, 3D-printed tubular scaffolds for vascular tissue engineering. *Procedia CIRP* **68**, 352–357 (2018). <https://doi.org/10.1016/j.procir.2017.12.094>
39. C. Best et al., Toward a patient-specific tissue engineered vascular graft. *J. Tissue Eng.* **9**, 2041731418764709 (2018). <https://doi.org/10.1177/2041731418764709>
40. “Full article: Customized 3D printed ankle-foot orthosis with adaptable carbon fibre composite spring joint.” <https://doi.org/10.1080/23311916.2016.1227022>. Accessed 22 Feb 2021
41. T. Serra, J.A. Planell, M. Navarro, High-resolution PLA-based composite scaffolds via 3-D printing technology. *Acta Biomater.* **9**(3), 5521–5530 (2013). <https://doi.org/10.1016/j.actbio.2012.10.041>
42. P.B. Dobrin, D. Hodgett, T. Canfield, R. Mrkvicka, Mechanical determinants of graft kinking. *Ann. Vasc. Surg.* **15**(3), 343–349 (2001). <https://doi.org/10.1007/s100160010078>
43. G. König et al., Mechanical properties of completely autologous human tissue engineered blood vessels compared to human saphenous vein and mammary artery. *Biomaterials* **30**(8), 1542–1550 (2009). <https://doi.org/10.1016/j.biomaterials.2008.11.011>
44. H.N. Patel, Y.K. Vohra, R. Singh, V. Thomas, HuBiogel incorporated fibro-porous hybrid nanomatrix graft for vascular tissue interfaces. *Mater. Today Chem.* (2020). <https://doi.org/10.1016/j.mtchem.2020.100323>
45. S. Sarkar, H.J. Salacinski, G. Hamilton, A.M. Seifalian, The mechanical properties of infrainguinal vascular bypass grafts: their role in influencing patency. *Eur. J. Vasc. Endovasc. Surg.* **31**(6), 627–636 (2006). <https://doi.org/10.1016/j.ejvs.2006.01.006>

46. M. Deutsch *et al.*, “Long-term experience in autologous in vitro endothelialization of infrainguinal ePTFE grafts,” *J. Vasc. Surg.*, vol. 49, no. 2, pp. 352–362., <https://doi.org/10.1016/j.jvs.2008.08.101> (discussion 362), 2009
47. B.B.J. Leal, N. Wakabayashi, K. Oyama, H. Kamiya, D.I. Braghirolli, P. Pranke, Vascular tissue engineering: polymers and methodologies for small caliber vascular grafts. *Front. Cardiovasc. Med.* (2021). <https://doi.org/10.3389/fcvm.2020.592361>
48. P. Fratzl, Cellulose and collagen: from fibres to tissues. *Curr. Opin. Colloid Interface Sci.* **8**(1), 32–39 (2003). [https://doi.org/10.1016/S1359-0294\(03\)00011-6](https://doi.org/10.1016/S1359-0294(03)00011-6)
49. J.L. Young, A.W. Holle, J.P. Spatz, Nanoscale and mechanical properties of the physiological cell–ECM microenvironment. *Exp. Cell Res.* **343**(1), 3–6 (2016). <https://doi.org/10.1016/j.yexcr.2015.10.037>
50. Physiology of Circulation | SEER Training, <https://training.seer.cancer.gov/anatomy/cardiovascular/blood/physiology.html>. Accessed 22 Feb 2021
51. N. T. Contributor, Vascular system 1: anatomy and physiology, *Nursing Times*, Mar. 26, 2018. <https://www.nursingtimes.net/clinical-archive/cardiovascular-clinical-archive/vascular-system-1-anatomy-and-physiology-26-03-2018/>. Accessed 22 Feb 2021
52. J.R. Levick, C.C. Michel, Microvascular fluid exchange and the revised Starling principle. *Cardiovasc. Res.* **87**(2), 198–210 (2010). <https://doi.org/10.1093/cvr/cvq062>
53. D.L. Donovan, S.P. Schmidt, S.P. Townshend, G.O. Njus, W.V. Sharp, Material and structural characterization of human saphenous vein. *J. Vasc. Surg.* **12**(5), 531–537 (1990)
54. M. Stekelenburg, M.C.M. Rutten, L.H.E.H. Snoeckx, F.P.T. Baaijens, Dynamic straining combined with fibrin gel cell seeding improves strength of tissue-engineered small-diameter vascular grafts. *Tissue Eng. Part A* **15**(5), 1081–1089 (2009). <https://doi.org/10.1089/ten.tea.2008.0183>
55. N. L’Heureux *et al.*, Human tissue-engineered blood vessels for adult arterial revascularization. *Nat. Med.* (2006). <https://doi.org/10.1038/nm1364>
56. T.R. Porter *et al.*, Direct in vivo evaluation of pulmonary arterial pathology in chronic congestive heart failure with catheter-based intravascular ultrasound imaging. *Am. J. Cardiol.* **71**(8), 754–757 (1993). [https://doi.org/10.1016/0002-9149\(93\)91024-c](https://doi.org/10.1016/0002-9149(93)91024-c)
57. K. Ma, S. Rozet, Y. Tamada, J. Yao, Q.-Q. Ni, Multi-layer nanofibrous tubes with dual drug-release profiles for vascular graft engineering. *J. Drug Deliv. Sci. Technol.* **53**, 100900 (2019). <https://doi.org/10.1016/j.jddst.2019.01.015>
58. D20 Committee, Test method for tensile properties of thin plastic sheeting, ASTM International. West Conshohocken
59. R. Johnson, Y. Ding, N. Nagiah, E. Monnet, W. Tan, Coaxially-structured fibres with tailored material properties for vascular graft implant. *Mater. Sci. Eng. C* **97**, 1–11 (2019). <https://doi.org/10.1016/j.msec.2018.11.036>
60. T. Yagi *et al.*, Preparation of double-raschel knitted silk vascular grafts and evaluation of short-term function in a rat abdominal aorta. *J. Artif. Organs* **14**(2), 89–99 (2011). <https://doi.org/10.1007/s10047-011-0554-z>
61. J. Johnson, D. Ohst, T. Groehl, S. Hettterscheidt, M. Jones, Development of novel, bioresorbable, small-diameter electrospun vascular grafts. *J. Tissue Sci. Eng.* **6**(2), 1–7 (2015). <https://doi.org/10.4172/2157-7552.1000151>